The influence of Ca/Mg ratio on autogelation of hydrogel biomaterials with bioceramic compounds

Anatolii Abalymov [a], Ekaterina Lengert[a,b,c], Louis Van der Meeren [a], Mariia Saveleva[a,d], Anna Ivanova[e], Timothy E. L. Douglas [f,g], Andre G. Skirtach[a], Dmitry Volodkin[h] Bogdan Parakhonskiy[a]*

a. Department of Molecular Biotechnology, Ghent University, 9000 Gent, Belgium.
b. First Moscow State Medical University (Sechenov University), Moscow 119992, Russia
c. Central Research Laboratory, Saratov State Medical University of V. I. Razumovsky, Ministry of Health of the Russian Federation, 410012 Saratov, Russia
d. Saratov State University, 410012 Saratov , Russia.
e. FSRC "Crystallography and Photonics", Shubnikov Institute of Crystallography, RAS, Moscow, Russia
f. Engineering Department, Lancaster University, Gillow Avenue, Lancaster LA1 4YX
g. Materials Science Institute (MSI), Lancaster University, United Kingdom

h. Nottingham Trent University, NG11 8NS, Clifton Lane, United Kingdom.

Total number words: 5426

Figures: 5

Tables: 2

Abstract

Hydrogels, which are versatile three-dimensional structures containing polymers and water, are very attractive for use in biomedical fields, but they suffer from rather weak mechanical properties. In this regard, biocompatible particles can be used to enhance their mechanical properties. The possibility of loading such particles with drugs (e.g. enzymes) makes them a particularly useful component in hydrogels. In this study, micro/nanoparticles containing various ratios of Ca^{2+}/Mg^{2+} with sizes ranging from 1 to 8 micrometers were prepared and mixed with gellan gum (GG) solution to study the in-situ formation of hydrogel-particle composites. The particles provide multiple functionalities: 1) they efficiently crosslink GG to induce hydrogel formation through the release of the divalent cations (Ca^{2+}/Mg^{2+}) known to bind to GG polymer chains; 2) they enhance mechanical properties of the hydrogel from 2 up to 100 kPa; 3) the most efficiently promoting cell growth samples were found to contain two types of minerals: vaterite and hydroxymagnesite, which enhanced cells proliferation and hydroxyapatite formation. The results demonstrate that such composite materials are attractive candidates for applications in bone regeneration.

Introduction

Tissue obtained from a patient's own body (autografts) and donors (allografts) are used to regenerate bone defects. Since autografting has several disadvantages (costs, patient pain, limited supply); allografting is used as an alternative[1]. However, this technique has limitations: uncertainty of disease transmission and biocompatibility. For these reasons, novel materials and methods are constantly sought, where an example is injectable materials[2,3]. The approach of the introduction of such materials is a minimally invasive one, and that results in lesser patient discomfort. In addition, outside of the body, the material is liquid but solidifies *in situ*. Thereby, the defect is completely filled, since the injected material can adopt the shape and size of a defect. Various applications of injectable materials have been reported, including those in dentistry [4]. Injectable hydrogels have been reported to be created based on proteins[5], but bone filling materials often also include bone cement consisting of calcium phosphates[6]. However, these materials have some drawbacks. For example, incorporation of biologically active components or

cells into these materials is not straightforward. Furthermore, cements, in particular, those based on hydroxyapatite, do not biodegrade sufficiently quickly to make room for new bone growth.

One of the novel approaches in drug delivery systems for bone defects is the use of hydrogels because of their unique properties, namely porous structure[7], biocompatibility[8], and biodegradability[9]. The porosity of hydrogels can be influenced by changing the crosslinking density. High biocompatibility is achieved due to a high water content and the structural similarity of a hydrogel to the native extracellular matrix. The biodegradability can be readily regulated via hydrolytic, enzymatic or environmental (e.g. pH, temperature) pathways. Hydrogels can deform easily and adapt to the required shape. However, there are also some limitations. The low tensile strength of many hydrogels limits their use in load-bearing applications and can result in the premature dissolution or dislocation of the hydrogel from a local targeted site[9]. Several strategies are available to increase the mechanical strength of the hydrogel. For example, it is possible to design hybrid materials[10] by incorporating various particles or networks[11], for example, bioglass particles[12] or hydroxyapatite particles[13]. Another solution is the incorporation of polydopamine, which enhances the mineralisability and hence stiffness of hydrogels[14]. Another example is mineralisation of hydrogels with zinc phosphate (by using alkaline phosphatase) [15] or mineralisation with carbonates, such as calcium carbonate ($CaCO_3$)[16], magnesium-enriched $CaCO_3$ and magnesium carbonate, facilitated by using urease[17]. Hence, the inclusion of carbonates represents a new solution for the enhancement of the mechanical properties of hydrogels.

Due to the highly porous structure of hydrogels, it is possible to load drugs into their matrix. Additional functionalization of such hydrogel with particles provides a higher loading capacity and controlled release of the payload[18–21]. Substances can be transported outside of the hydrogel by diffusion while maintaining the cell viability[22]. By the same process, toxic and undesirable products can be removed[23]. Also, such biologically active substances as calcium phosphates and calcium carbonate particles or capsules can be incorporated to stimulate cell proliferation required for bone growth. These particles can be loaded with low-molecular-weight drugs such as antibiotics, photosensitizers, or high-molecular-weight enzymes and proteins[24,25].

Calcium carbonate particles in the vaterite phase have become one of the most popular cores for templating polymer-based capsules. $CaCO_3$ particles have several benefits: a simple preparation procedure[26,27], low costs, good biocompatibility[28], and mild decomposition conditions[29]. Overviews of $CaCO_3$-based encapsulation have been presented in reviews [30,31]. The main advantage of $CaCO_3$ is the possibility of controlling the size and shape of the particles during their synthesis[26,27,32–34]. Because the synthesis of $CaCO_3$ particles is sensitive to reagent concentration, temperature, intensity, and duration of stirring of the reaction mixture[35], these parameters need to be controlled throughout the reaction. The porous structure of the vaterite allows immobilization of various amounts of such drugs as ibuprophen [36,37], cyclodextrin[38], photosensitizers [29,39,40], doxorubicine [41–43], enzymes [21,24], *etc*. Carbonate particles are also used to synthesize alginate hydrogels. Kuo and Ma reported preparation of alginate hydrogels using both $CaCO_3$-GDL and $CaCO_3$-GDL-$CaSO_4$ systems[44]. Porous alginate gels can be formed using pure $CaCO_3$ particles (no additives), which: (i) supply calcium ions, (ii) provide the structural material, and (iii) can be used as containers to load pores with molecules of interest within the single step of gel fabrication[45–48]. Variation of the synthesis parameters allows the preparation of particles in the size range from 300 nanometres to 10 micrometers. Furthermore, metastable vaterite particles can re-crystallize in an aqueous solution to calcite (which has a lower solubility)[49], while some coatings, including layer-by-layer functionalization[50–52] can be used to control that process.

The gelation of the anionic polysaccharide gellan gum (GG) can be introduced using microparticles and bioactive glasses, providing a source of ions for cell homeostasis. In this regard, $Mg^{2+}$is the key regulator of the balance between osteoclast and osteoblast differentiation[53,54], adhesion[55] and bone formation [56], while calcium ions are an active component of hydroxyapatite production[57], and a structural component of bones. However, limited attention has been devoted to the study of hydrogels with the presence of both of these ions. Carbonate particles can serve as delivery vehicles for the slow release of calcium and magnesium (Mg) ions to crosslink anionic polysaccharides such as GG to form homogeneous hydrogels. Carbonate microparticles containing Ca and/or Mg can be formed easily by mixing Ca^{2+}, Mg^{2+}, and CO_3^{2-} ions at different concentrations [58]. For example, Douglas *et al* have reported the gelation of GG using magnesium/calcium/zinc carbonates [59]. The presence of such Ca and Mg ions in the final composition of the materials for bone regeneration has been shown to have a strong impact on cell proliferation, but, to the best of our knowledge, the influence of particles with various relative ratios of Ca/Mg has not been studied.

To form bioactive materials based on the hydrogel with incorporation of the bio ceramic particles already reported in 2D structure via in vivo synthesis of the particles [57,60–62], it was shown that the special alignment for the gel molecules is required and that the particles should be well incorporated in a gel to provide centres for the cell adhesion[16] and specific mechanical properties. But design of such materials in 3D matrix is still a big challenge.

In this study, we have designed novel types of particles based on calcium and magnesium carbonate and subjected them to detailed physiochemical characterization. We studied the influence of the ratio of Ca and Mg ions in the reaction mixture on the properties of the particles, i.e. on their size, shape, reaction yield, crystallographic structure and composition, and their influence on the formation of injectable hydrogel-particles composites, which can work as a 3D matrix for osteoblastic cells and promote theirproliferation and hydroxyapatite formation, which is one the most important factors for ossification.

Experimental Section

Materials and reagents Sodium carbonate (Na_2CO_3), calcium chloride ($CaCl_2$), magnesium chloride ($MgCl_2$), calcium carbonate ($CaCO_3$), GG (Gelzan™ CM), and ethylene glycol were all purchased from Sigma-Aldrich without any further purification. Ethanol ($C_2H_6O_2$) was purchased from Chem-Lab. In all experiments, ultra-pure water with a resistivity higher than 18.2MΩ cm was used.

Synthesis of (Mg-Ca)CO_3 particles in water

Particles were synthesized by mixing 2 mL of 0.33 M Na_2CO_3 with 2 mL of mixture solution Ca^{2+}/Mg^{2+} (as mixture of 0.33M $CaCl_2$ and 0.33M $MgCl_2$) having volume ratios of 0:100; 25:75; 50:50; 75:25; and 100:0 which correspond to sample numbers 1, 2, 3, 4, and 5, respectively. The mixture was agitated using a magnetic stirrer at 750 RPM (Rounds per Minute) for 1 minute at room temperature. Afterward, the mixture was centrifuged for 5 minutes at 3000 RPM in 2 mL tubes. The supernatant was removed, and the pellet was washed twice with ethanol (70%) and centrifuged (3000 RPM, 5 min.) after washing. The samples were dried for 10 hours at 70°C for storage.

Characterisation

Particle morphology characterisation was performed by using images obtained by scanning electron microscopy (SEM) and transmission/scanning transmission electron microscopy (TEM/STEM). SEM measurements were performed with MIRA II LMU (Tescan) at an operating voltage of 15 kV, in secondary electron and backscattering electron modes. Magnification was varied from 100x to 40000x. Samples were prepared by drying a drop of the aqueous suspension of microparticles on a silicon wafer.
The size distribution of the calcium carbonate particles was obtained by post-processing and image analysis of SEM micrographs with ImageJ software (NIH, http://rsb.info.nih.gov/ij/). At least 100 measurements per sample were performed.
Powder X-ray diffraction analysis of the polycrystalline samples was performed with a Rigaku Miniflex-600 diffractometer (Rigaku Corporation, Tokyo, Japan). The XRD data were recorded using Cu-Kα radiation (40 kV, 15 mA, Ni-Kβ filter) in the 2θ range 10–80° at a scan speed of 1°/min. The crystalline phases were identified by using an integrated X-ray powder diffraction software (PDXL: Rigaku Diffraction Software) and ICDD PDF-2 datasets (Release 2014 RDB).
An FTIR spectrometer, Bruker (VERTEX 70) in the ATR reflection mode, was used to obtain infrared spectra of different types of particles. The spectra were recorded in the range of 150-4200 cm^{-1}. The spectrum of each sample was measured 15 times, and the average spectrum was calculated.
ANOVA (Analysis of variances) is an analysis tool to test whether there are statistical differences between the means of two groups in an experiment. This analysis was performed with SPSS. One-way ANOVA analysis was performed to compare the yield with a significant difference for $p<0.05$.
A rheometer (AR-1000 N, TA Instruments) was used to study the viscoelastic properties of the hydrogels. The rheometer consists of a stainless steel plate and an acrylic cone of 40 mm. The storage (G') and loss modulus (G") was recorded at 22°C with a frequency of 1 Hz and an angular frequency of 6.283 rad/s.

Preparation of the hydrogels

GG was dissolved in double-distilled water at a concentration of 0.875% (w/v). The solution was autoclaved for 15 minutes at 121°C. Hydrogels prepared in this work contained 4%, and 30% of the particles (table1). The preparation was carried out in 2 mL reaction tubes (Greiner Bio-One). 300 µL distilled water was added to the to the presynthesized particles. The particles were dispersed using an ultrasonic bath (Sonorex Super 10P, Bandelin) for 30 seconds at room temperature. Afterward, 500 µL of GG was added and mixed with the particles by shaking the reaction tubes.

Table 1. Particles' synthesis parameters and their amount added to the corresponding gel.

Particle's name	Ca^{2+}/Mg^{2+} ration in a particles reaction mixture	Gel's name	% by of the particle added to the gel
B1	100:0		--
B2	75:25	GG30%-2	30%
B3	50:50	GG4%-3	4%
B4	25:75	GG4%-4	4%
b5	0:100	GG4%-5	4%

Mechanical tests

Mechanical tests were performed using a universal testing machine. Mechanical stiffness of gels was investigated using a Universal Test Machine, LS1 (1 kN) Material Tester from Lloyd Instruments, Inc. (Ametek). A 50 N load cell was used to make a 1 mm indentation in samples with a preload of 0.03 N. Probing was performed using cylindrical posts of 2.5 cm. The indentations were

conducted to maintain minimal strain and to avoid the influence of the substrate. Five replicates were used for each sample. To determine the Young's modulus, a dip of 2 mm was made into the sample (50% of one gel layer). For all Atomic Force Microscopy (AFM) experiments the Nanowizard 4™ (JPK instruments GmbH/Bruker) was used. Topographical images were acquired in the JPK QI® mode using DNP-S10 cantilevers (Bruker, force constant: 0.35 N/m, radius of curvature < 10 nm). All force curves were acquired in contact mode with the same probes and using setpoints ranging from 2-6 nN. To obtain the Young's modulus from the force curves a Hertz model adjusted for colloidal indenters was used, in the JPK data processing software (JPK, Germany)[63].
To gain information on the viscoelastic properties of hydrogels, microrheological measurements were performed using DNP-S10 chips. In these measurements, the force reaction toward small amplitude oscillating forces (at low frequencies) that are applied at the surface are analyzed. The oscillations in the experiments were performed with an amplitude of 50 nm at frequencies ranging between 10 and 100 Hz. Calculations of the storage and the loss moduli were performed in JPK data processing software, based on calculations adapted from a previous paper on microrheological measurements on live cells [64]. To accommodate for influences originating from the cantilever's geometry, first, the deviation from 90° phase shift in the liquid environment and the hydrodynamic drag coefficient was calculated and incorporated into the measurements. Fitting the microrheological data to the soft glassy rheology model was performed by non-linear fitting in OriginPRO 2021[65].

Cell experiments

For testing biological compatibility of hydrogels, the pre-osteoblastic cell line MC3T3-E1 (ATCC) was used. Cells were cultured in MEM-alpha glutaMAX-1™ (Sigma-Aldrich, Cat. No. 32561- 029) supplemented with 10% FBS, 2 mM glutamine, and 100 µg/mL penicillin/streptomycin. The medium was replaced every 3 days, and the cells were maintained in a humidified incubator at 5% CO_2 and 37°C with 5% CO_2 (Innova CO-170, New Brunswick Scientific). Cells were used in passages 2–6.
The viability of MC3T3-E1 cells on various hydrogel-particles composite surfaces was determined by AlamarBlue (Thermo Fisher, Product no. DAL1025). 50 µL of GG solution was added to each well of a 96-well plate. After that, we added $5*10^4$ cells per well and crosslinked the hydrogels by adding mineral particles with concentrations: 30% for 25%:75% Ca:Mg ratio and 4% for particles synthesized in the presence of salts with Ca:Mg ratio 50%:50%, 25%:75, and 0%:100% and incubated overnight at 37 °C under 5% CO_2. Hydrogel solution was prepared in sterile condition of a laminar box, particles were sterilised by 70% ethanol. In the last step, 10 µL of PrestoBlue reagent was added to each well for 3 hours, and then the fluorescent (540/610 nm) intensity was measured by a spectrophotometer (Infinite F200 PRO). The cell viability was studied at the first and third days.
The cytotoxicity of carriers was analyzed by a lactate dehydrogenase assay (LDH). MC3T3-E1 cells were mixed with hydrogel and particles as previously described. As a negative control, 1 mM of Triton X-100 was added to the culture medium. After 1 and 3 days of incubation with samples, cultural media was replaced with a new 96 well plate; an LDH assay was conducted following the manufacturer's instructions. The absorbance measured at 690 nm was subtracted from the absorbance at 490 nm to compensate for the sample turbidity.
For cells' visualization a Nikon TI (Nikon, Japan) fluorescence microscope with 10X objective and appropriate filters were used. After 1 and 3 days of incubation inside hydrogel matrix, cell layers were then stained with Calcein AM (Thermo Fisher, Product no. C1430) and Propidium Iodide (Thermo Fisher, Product no. P1304MP). Cells were incubated with a medium containing 0.1 mM of the reagents for 15 min at RT.
Cells were cultured for 1 and 3 days in an osteogenic medium (primary medium supplemented with ascorbic acid, sodium glycerophosphate, and dexamethasone (50 µg/mL, 0.1 µM, and 10 nM, respectively)), and at each time point they were harvested by trypsin-EDTA and collected by centrifugation. The extent of mineralization was determined using an Osteoimage Mineralization Assay (Lonza. Belgium.cat. no. PA-1503). After each culture time point, the hydrogels were washed with 1× PBS before being fixed with 4 % (w/v) PFA for 20 min at RT. Samples were subsequently washed further twice (5–10 min each) with osteoimage wash buffer and then incubated with 0.1 mL staining reagent, in the dark for 30 min. After incubation, gels were washed three times (5 min each) with wash buffer before. To quantify the extent of mineralization, washed samples were resuspended in 0.2-µL wash buffer and their fluorescence was determined in a fluorescent plate reader (Infinite F200 PRO) at a 492/520 nm ratio. Two independent assays were performed, again in triplicates.

Results and Discussion

We demonstrated a new type of calcium/magnesium carbonate particles with characteristics suitable to create in-situ forming hydrogel-particles composites. Different shapes of particles were created by varying the Ca^{2+}:Mg^{2+} ratio, as demonstrated in Fig. 1a. The high (more than 50%) content of calcium ions in the reaction mixture leads to the formation of the spherical particles. The presence of the magnesium stimulates the formation of paired particles and an amorphous phase of $CaCO_3$.

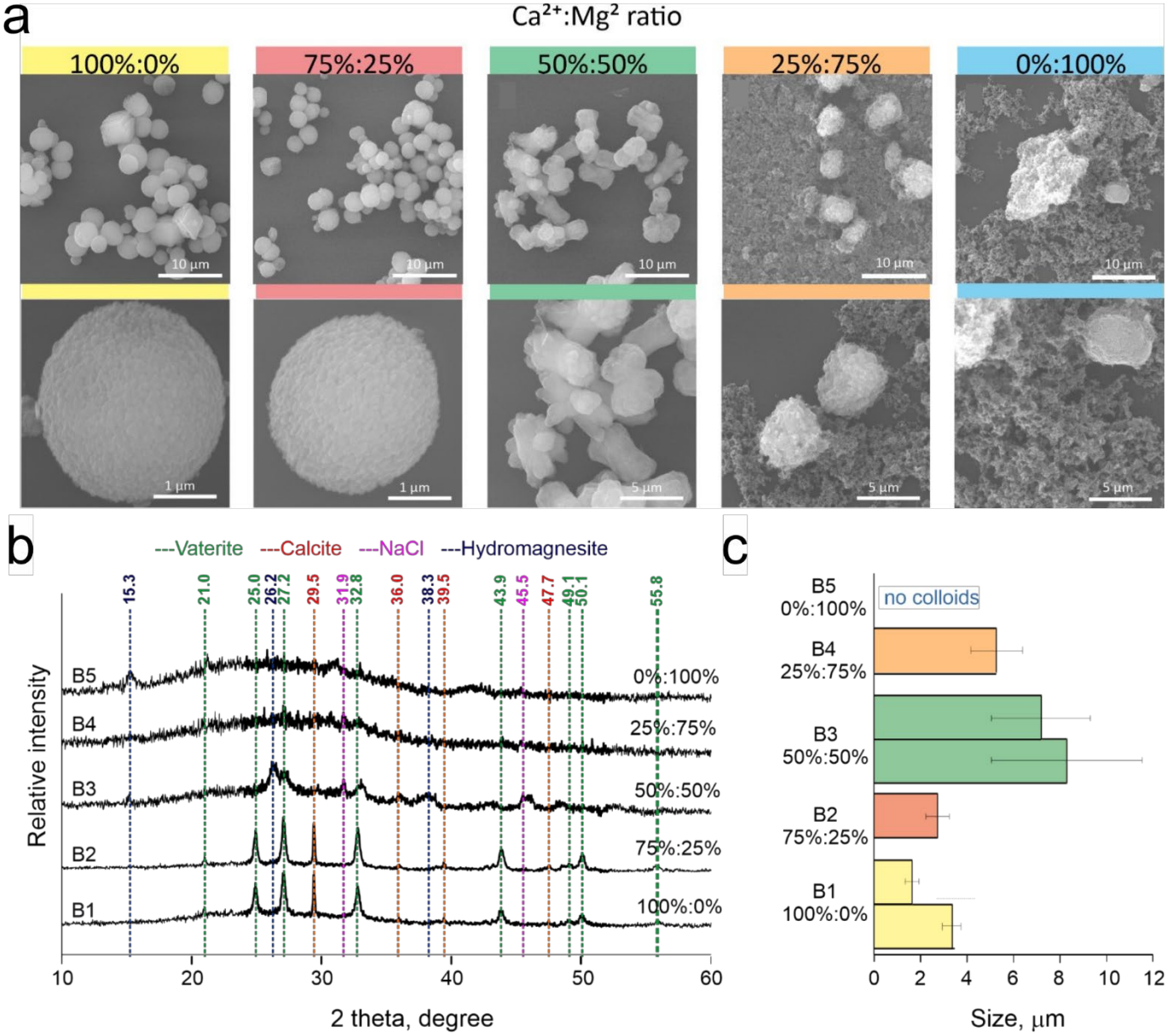

in reaction mixture ranging from 100%:0% to 0%: 100%. B) XRD spectra for particles synthesised with different Ca^{2+} and Mg^{2+} ratios. (B1 for 0:100, B2 for 25:75, B3 for 50:50, B4 for 75:25, B5 for 100:0). c) Size distribution of the obtained particles with the vaterite structure for samples B1, B2 and B3. Sample B1 and B2 have a bimodal distribution reflected as two (green) bars in the bar chart.

If the amount of calcium is lower than 50%, amorphous particles are formed. All samples consist of vaterite and/or calcite particles, independent of the reaction time and Ca^{2+}:Mg^{2+} ratio. Hydromagnesite particles are formed at a higher Ca^{2+}:Mg^{2+} ratio.

The particle structures were characterised using X-ray diffraction (Fig. 1b). Particles (samples 1 and 2 show peaks at 2θ values 21.0; 25.0; 27;2; 32.8; 43.9; 49.1; 50.1, and 55.8 degrees; all corresponding to vaterite [66]. Also, calcite peaks occur in these samples at 29.5; 36.0; 39.5, and 47.7 degrees. This suggests that in both samples, vaterite and calcite are present. In the SEM images, however, calcite particles are only detected in samples 1 and 2, which can be assigned to the fact that all the samples could be covering sample 3 peaks occur at 27.2 and 32.8 suggesting the presence of vaterite and also at 36.0 the peak corresponding to calcite is shown. In addition to these peaks, other peaks at 31.9 and 45.5 are present, which are characteristic of NaCl. Also, typical hydromagnesite peaks can be found at 15.3 and 38.3 degrees [67] for samples 3, 4, and 5. Samples 3, 4, and 5 show a quite broad peak at approximately 26.0, suggesting the presence of an amorphous phase which is correlated with SEM images (Fig. 1a).

For spherical particles, the diameter of the particles was measured. For the elliptical and paired particles, the axial and radial sides were determined. The size of the particles, analysed based on the SEM images (Fig. 2b), ranged between 1.6 and 8.2 µm. The elliptical particles show a size close to 8 µm and an elongated elliptical shape.

The reaction yield from Ca:Mg ratio 100%:0% (60 %) is lower than the reaction yield from the particles synthesised by Svenskaya *et al.* (74% with a magnetic stirrer and 85.9% with ultrasonic agitation)[26]. The analysis shows that Ca^{2+}:Mg^{2+} ratio does not significantly influence the reaction yield and thus has no effect on the ion distribution. These particles were used as components for the preparation of hybrid hydrogels, as described in Fig. 2a. In step 1 we synthesized particles with different ratios of Mg2+ and

Ca^{2+} ions. In step 2, particles were added to the GG solution and well mixed for good particle distribution (Step 3). GG is a polysaccharide which multivalent ions can crosslink. After particles enter the aqueous medium of the GG solution, they start to release Mg^{2+} and Ca^{2+}, which crosslink GG molecules in 20 min at room temperature (Step 4). Photos of the actual crosslinking process of GG solution by particles are shown in Fig. 2b.

Particles containing only Ca^{2+} are not capable of crosslinking GG, presumably due to a slow and/or insufficient release of Ca^{2+} ions, while particles containing either Mg^{2+} or both Mg^{2+} and Ca^{2+} are capable of crosslinking GG. Results show that the gelation time increases if either the particle concentration increases or Ca^{2+}:Mg^{2+} ratio decreases

.

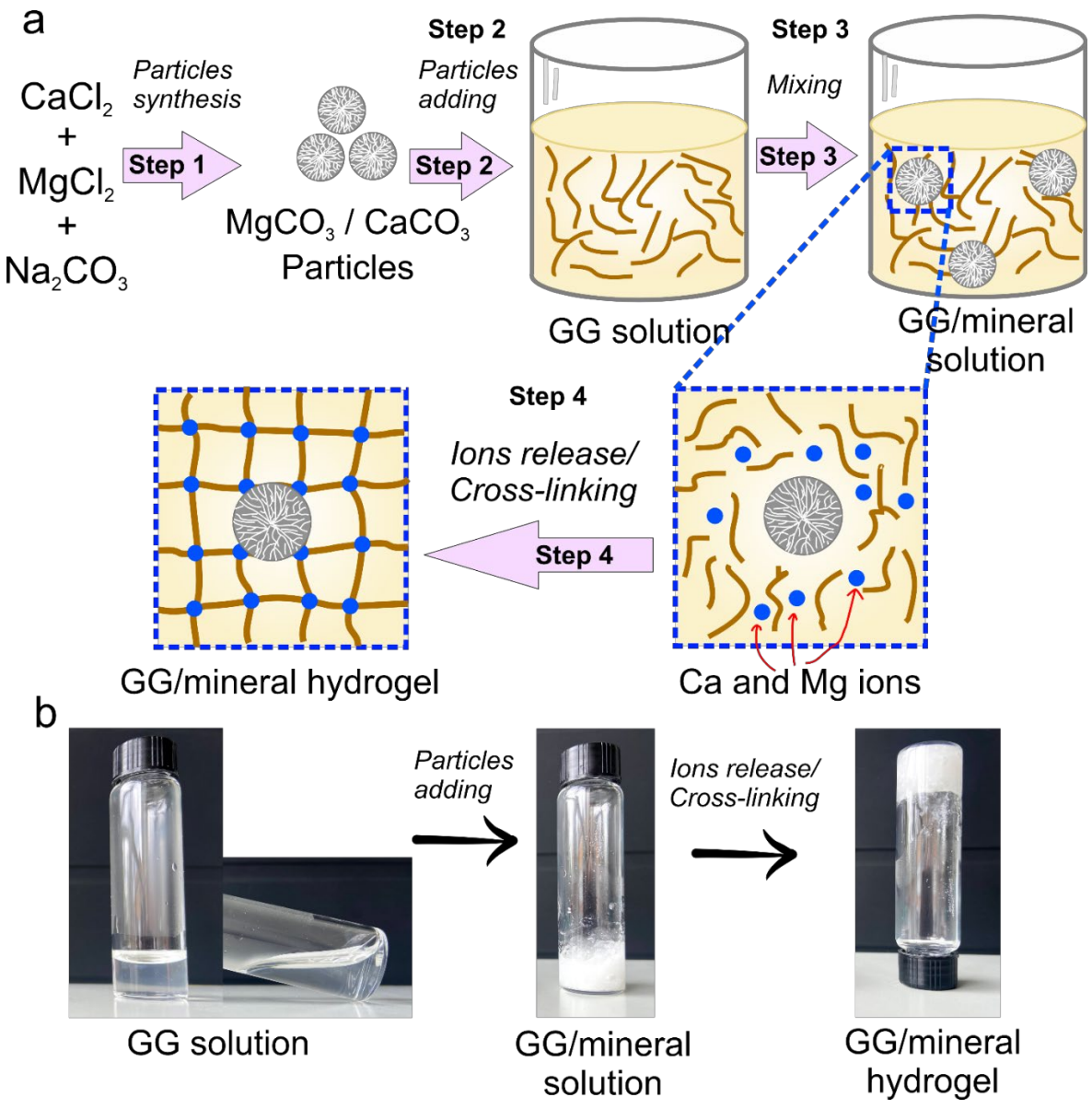

2. SEM (scanning electron microscopy) overview (top row), and magnified (bottom row) SEM images, corresponding to each above-located overview panel, of particles with different Ca^{2+} : Mg^{2+} ratios in reaction mixture ranging from 100%:0% to 0%: 100%.

Rheometry results in Fig. S3 show that the storage modulus of the hydrogel increases with increasing particle concentration, whereas at a specified particle concentration, the mechanical stiffness increases with decreasing the Ca^{2+}:Mg^{2+} ratio. Fig. S1 shows the average storage modulus as a function of time determined from three measurements for each sample. The average and the standard deviation are calculated for storage modulus and time (Supporting Information, Table S1).

The influence of the crystallographic structure of the particles (vaterite, calcite, hydromagnesite, magnesian calcite, and amorphous) was studied for hydrogels containing a specific type and concentration of pre-synthesized particles: a) 4% (by mass) particles with various Mg^{2+} percentages (50%, 66.6%, and 100%), and b) 30% of particles with an Mg^{2+} percentage of 33.3% (Fig. 3); thus, the highest concentrations, at which the gel forms a stable uniform structure and is not split into separate parts. FTIR spectra showed the presence of calcite, but not vaterite, in all hydrogels. However, hydromagnesite particles were only found in the hydrogel consisting of 4 % particles with 100% magnesium. First, ANOVA analysis was performed, with $p<0.05$ considered as

significant, in order to compare hydrogel strength for different types of hydrogels. According to ANOVA analysis, no significant difference was detected only between hydrogels-particles composite with 4% of particles synthesis from 0%:100% and the same amount of the 50%:50% Ca:Mg particles, which suggests that if the particle concentration is increased from 2 to 4 %, the hydrogel strength increases significantly.

For the following studies, the concentration of the particles was adjusted so that the gelation time was 30 min. The detailed studies of the mechanical properties of the hydrogels were performed by atomic force microscopy with probe size 30 nm and an universal testing machine with probe 10 mm (Fig. 3a). The studies included measurements of the Young modulus, compression strain and results of the microrheology measurements (complex storage modulus, and complex shear loss) and their coefficient in the simulation (scaling factor) and (matrix agitation). Based on the UTM data, macro-mechanical properties (MMP) Young's modulus values of samples were in the range between 80 and 289 kPa but nano mechanical properties obtained by AFM analysis were in the range 100-300 kPa (Fig. 3b). In force mapping (Fig. 3c), the gels demonstrated a homogeneous distribution with alternating weaker areas (in the range up to 10 kPA) and stronger hydrogel (in the range 100-150 kPa) areas. Various compositions of particles were used for gelification. It wasrevealed that particles containing 75%:25% Ca:Mg provide the strongest Young's modulus and thus significantly (based ANOVA test) better mechanical properties (Fig 3d), due to the presence of the amorphous phase and particles. In comparison, the shear loss (Fig 3e) of the 50:50 ratio (green curve) demonstrates a better result with respect to the rest of the gels.

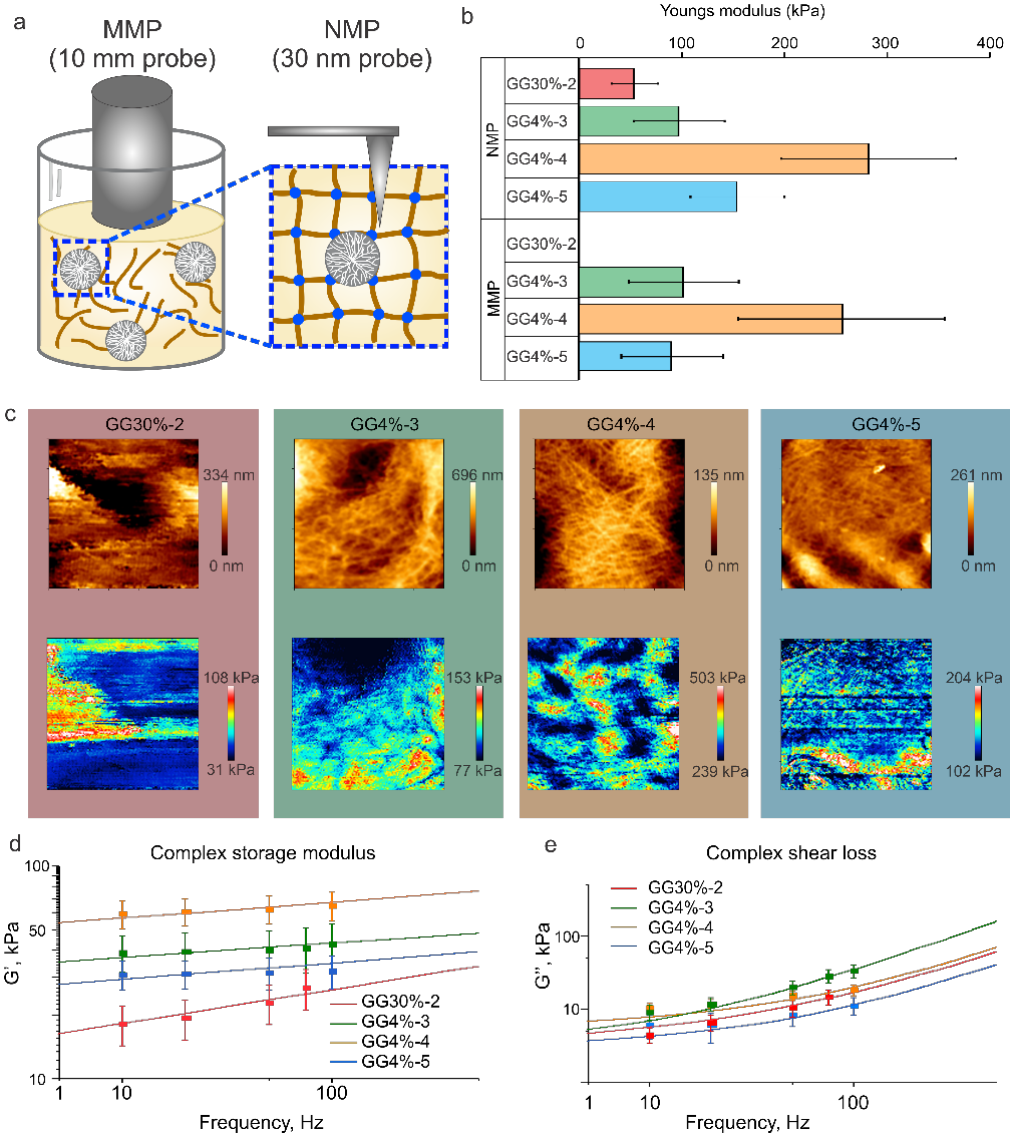

Fig. 3. a) Schematic of the gel formation; b-e) Mechanical properties and topography images of GG gelified with various types of particles: red -30% of the second type B2 sample of the particles (GG30%-2), green- 4% of the 3rd type of the particles (GG4%-3), orange- 4% of the 4th type of the particles (GG4%-5), green- 4% of the 5th type of the particles (GG4%-5), b) Young's modulus measured by the universal testing machine. c-e) c) Atomic Force Microscopy data for topography: upper panel and force map bottom panel, d -e) data for microviscosity measurements: e) complex storage modulus, f) the complex shear loss.

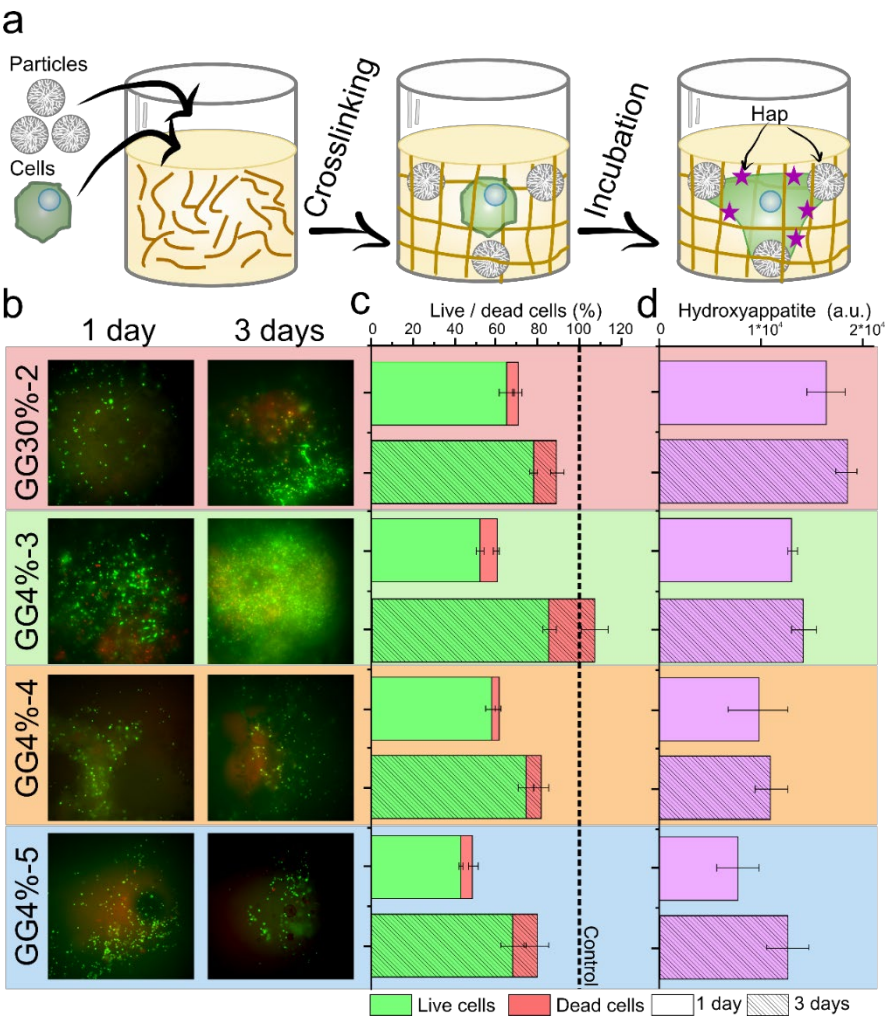

Fig. 4. Results of the cell viability measurements normalised to the control cells (plastic) of the hydrogel samples which were performed at different time points: solid filled bars - 1st day of incubation; striped fill bars - 5th day of incubation; the horizontal line represents the toxicity data for average normalised control cells without any additives. The statistical analysis was performed by repeating analysis of 5 independent samples using the ANOVA test. ^ denotes a significant difference of the cell viability of the gels for day 5 with respect to day 1, * denotes differences with respect to the control.

AFM morphology and mechanical analysis was performed on all the samples (fig 3d,g). From this analysis, it is seen that GG30%-2 has the lowest Young's modulus. When analysing the morphology, no clear mesh structure can be observed which explains the lower Young's modulus in that case. The GG4%-3 gel shows a clear network structure with larger pores. This also translates into a higher Young's modulus compared to that for GG30%-2. A slightly higher Young's modulus is noticed in sample GG4%-5, which is also supported by observation that the fibres are more tightly packed (smaller pores, compared to sample GG4%-3). The sample with the highest Young's modulus, i.e. GG4%-4, shows the most tightly packed mesh (very straight fibres with small pores), thus resulting in the highest Young's modulus. All samples show a homogeneous force map meaning that there is a uniform gel/mesh structure present.

shown in the table 2 below. It can be noticed that the green sample has the highest loss tangent meaning that from all the samples it exhibits the most viscous behaviour. It is noteworthy that this value (0.78 still indicates quite an elastic sample, since the value of the loss tangent varies between 0 (perfectly elastic) and +∞ (perfectly viscous).

Table 2 Loss tangent at 100 Hz for the hydrogel samples functionalized with particles.

Sample	Loss tangent at 100 Hz
GG30%-2	0.556577
GG4%-3	0.784975
GG4%-4	0.283475
GG4%-5	0.353528

From cell experiments, it can be concluded that samples GG30%-2 and GG4%-3 hydrogels show the most promising results. For conducting the experiments, osteoblastic cells were mixed in GG with particles simultaneously, as presented in figure 4a.

Fluorescence images after 1 and 3 days of incubation show that cells in the hydrogel matrix have different fluorescence levels. The increasing green fluorescence of Calcein Am indicates that the number of living cells in the hydrogel increased, as can be seen from comparing photos of GG4%-3 hydrogel after 1 and 3 days of incubation. Samples GG4%-4 and GG4%-5 did not show such progress in cell proliferation. These results were comparable with Alamar blue and LDH experiments (Fig.4c).

Figure 4c shows that cells cultured inside GG4%-3 have the highest proliferation rate compared to days 1 and 3: 52.2 and 85.8%, respectively, but at the same time the highest death rate (21.3% after 3 days) was observed. Also, cells inside GG4%-4 hydrogel have a high proliferation rate (from 42.6 to 68%), but the deficient percent of an alive cell after the first day of incubation makes this sample partly cytotoxic limiting their application in biomedicine. [69]

Figure 4d shows the results of the hydroxyapatite deposition test. Hydroxyapatite is an essential mineral of bones, which is usually produced by osteoblastic cells in their livelihoods. The rate of hydroxyapatite crystal formation by osteoblasts is one of the parameters for determining the possibility to use the biomaterial for bone tissue engineering via the following reaction:

$$CaCO_3 \xrightarrow{H^+} Ca^{2+} \xrightarrow{PO_4^{3-}} \begin{cases} Ca(H_2PO_4) * H_2O \\ \downarrow Ca^{2+} \\ CaHPO_4 * 2H_2O \\ \downarrow \\ CaHPO_4 \end{cases} \xrightarrow{Ca^{2+}} Ca_{10}(PO_4)_6(OH)_2$$

Ca^{2+} and PO_4^{3-} ions are two major components of hydroxyapatite. Both ions (Ca^{2+} and PO_4^{3-}) are present in the cell growth media in the form of calcium chloride (264 mg/l), sodium phosphate (158 mg/l) and glycerol phosphate (0.03 mg/L), which are initially present in equilibrium in the medium. The calcium carbonate particles occurring as the vaterite metastable polymorph in the composite hydrogel system are a major source of the calcium ions. On the other hand the phosphorus ions are synthesized in cells in the form of polyphosphate. [70] Finally, Ca^{2+} ions of polyphosphate undergoes hydrolysis through a alkaline phosphatase (ALP)-mediated enzymatic reaction, resulting in the liberation of both orthophosphate and Ca^{2+}. Calcium phosphate precipitates in the extracellular space onto the calcium carbonate bio seeds under formation of calcium carbonated apatite. Initially, cells have osteocalcin-protein that connects the membrane and hydroxyapatite crystals, which are synthesized on the surface of osteocalcin. This usually occurs due to carbonic anhydrase driving/accelerating the formation of bicarbonate, which reacts to carbonic acid and finally undergoes precipitation to calcium carbonate. Our system contains a large number of calcium ions and carbonate anions, which are constantly released by the particles inside the hydrogel. This significantly accelerates the synthesis of hydroxyapatite crystals on the cell surface. Our system tried to apply all critical parameters for successful ossification: a 3D matrix and the presence of two essential ions – Ca^{2+} and Mg^{2+}. $CaCO_3$ is the primary material for hydroxyapatite formation, which connects with the cell membrane through the osteocalcin protein. Mg^{2+} ions accumulate in bone tissue and are concentrated on the hydrated surface layers of apatite crystals instead of being incorporated into the lattice structure of bone crystals.

The plot of hydroxyapatite formation is presented in Figure 4d. From this image, it can be concluded that osteoblasts in GG30%-2 hydrogel have produced most of the Hap crystals on the third day compared to the other samples, suggesting that Ca^{2+} ions are more critical for the ossification process[71].

Cells viability, death rate, and Hap production depend on different factors. In our system, we tried to check the influence of mechanical properties of the obtained hydrogels. The proliferation of cells better inside GG4%-3 does not depend on the Young's modulus of the hydrogel matrix (Fig. 5a). However, the Young's modulus of hydrogels has an apparent influence on hydroxyapatite production. The fluorescent signal from hydroxyapatite crystals increases with decreasingYoung's modulus (Fig. 5b).

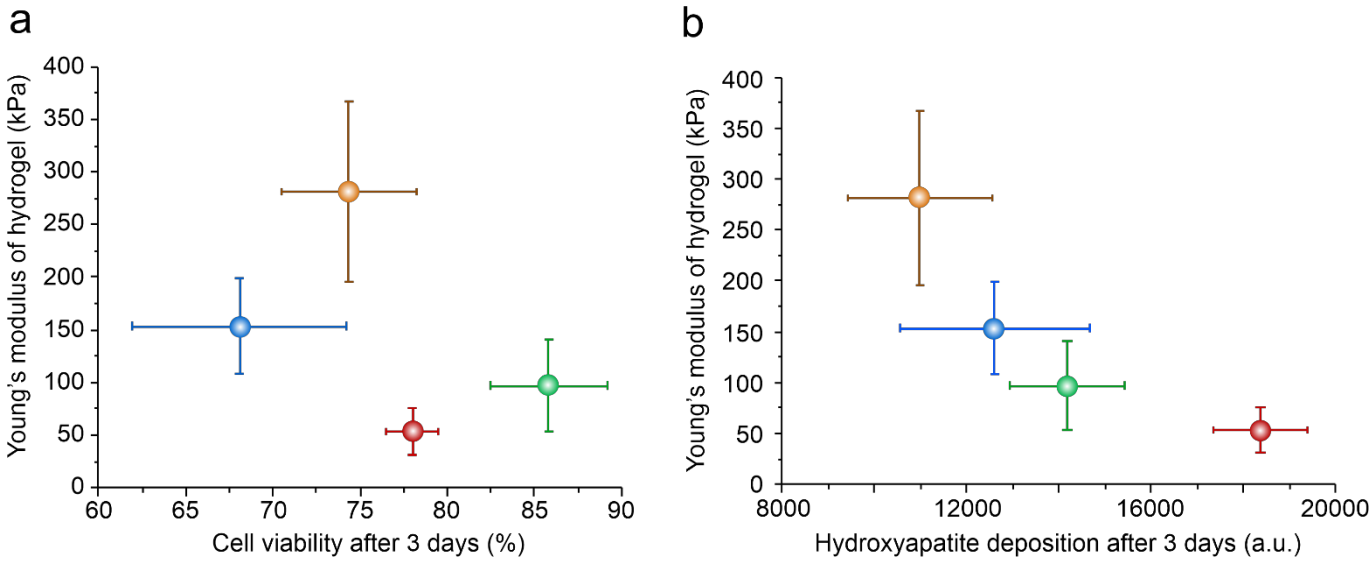

Fig.5. Correlation of the Young's modulus of hydrogel matrix and (a) cell viability after 3 days of incubation (b) hydroxyapatite formation after 3 days of incubation. .

The mechanical properties of the final hydrogels are shown in Fig. 3. The Young's modulus for all types of gels is situated in the range of 0.1-0.4 MPa, which falls into the range suitable for osteoblastic cell growth [72].
To study the influence of these gels on cell growth, cell availability tests were performed (Fig. 4). Almost all groups (except GG/30%-2 and GG/4%-5) of gels demonstrate intensive cell growth during 5 days, i.e. up to 3 times better than that of the control cells grown on the plastic well plate. The hydrogel-particles composite with higher vaterite percentage (GG/30%-2) has no appreciable effect on the cell growth. In the opposite case, the gels with 50/50 magnesium to calcium content (GG/4%-3) demonstrate a significant increase in the number of cells. This can be explained by the highest viscosity of gels resulting in improved mechanical properties, in accordance with Fig. 3.
This study proves the concept of applying composite carbonate nano- and micro-particles for tailor-made assembly of hydrogels with enhanced mechanical properties and the potential capacity to host bioactive molecules pre-encapsulated into the carbonate particles.

Conclusions

Isotropic (spherical and cubic) and anisotropic (elliptical) inorganic $CaCO_3$-$MgCO_3$ particles have been synthesised by controlling the crystallisation reaction involving mixing the corresponding salts at various calcium/magnesium ratios. Possibilities of forming injectable hydrogel materials containing composite particles synthesised with various ratios of Ca^{2+} to Mg^{2+} ions: 0:100, 25:75, 50:50, 75:25, 100:0 have been investigated revealing conditions for controlling the gelification process in the time interval from minutes till hours and with the mineral contents from 4% to 30%. It was found that pure vaterite particles (Ca/Mg=100:0) do not induce gelation, but in contrast, Ca/Mg=75:25 particles allow the formation of gels containing around 30 % of the mineral phase. Increasing the percentage of Mg^{2+} in the particle synthesis (Ca/Mg=50:50; 25:75; 0:100) allows the synthesis of particles containing a higher content of the amorphous phase, and, as a result, a better capability to form a gel, where a particle content of approximately 4% is already sufficient to induce the formation of a stable gel within 20 minutes. All gels have the macro Young's modulus between 2 kPa and 7 kPa The local Young's modulus was measured by AFM from 50-100 kPA (for Ca/Mg=75: 25, 50:50; 0:100) and 150 for (Ca/Mg=25:57) ratio. The samples with 50:50 and 25:75 Ca/Mg ratios demonstrate a higher cell viability and hydroxyapatite production than that of the control cells on a plastic surface or other hydrogels.
The gels with hydromagnesite particles are significantly better for cell growth compared to other formulations measured after 3 days. For potential future applications, antibacterial properties of such hydrogels can be enhanced by natural compounds [73,74]. Such a synthetic method provides a novel way for the direct solution-based growth of porous particles of different shapes, sizes, and compositions. This research opens new avenues to formulate self-hardening multifunctional hydrogels for biomedical applications, especially for developing injectable reconstruction materials for filling micro-scaled defects in bone tissue.

Author Contributions

The manuscript was written through the contributions of all authors. All authors have given approval to the final version of the manuscript.

Acknowledgements

We would like to thank V. Atkin (Saratov State University, Saratov, Russia) for SEM measurements. We thank the ERA-NET Rus Plus program for support in the framework of the project "Fabrication and investigation of new hybrid scaffolds with the controlled porous hierarchy for bone tissue engineering" (Intelbiocomp G0D7115N). BP thanks the Research Foundation Flanders (FWO) (524618N), Belgium. AGS acknowledges support the fund for Scientific Research (FWO) Flanders (I002620N, G043219N) and the Special Research Fund (BOF) of Ghent University (IOP 01/O3618, BAS094-18, BOF14/IOP/003).). XRD mesearments were performed using the equipment of the Shared Research Center FSRC "Crystallography and Photonics" RAS and was supported by the Russian Ministry of Education and Science.

Conflicts of interest

"There are no conflicts to declare".

References

[1] K.S. Griffin, K.M. Davis, T.O. McKinley, J.O. Anglen, T.M.G. Chu, J.D. Boerckel, M.A. Kacena, Evolution of Bone Grafting: Bone Grafts and Tissue Engineering Strategies for Vascularized Bone Regeneration, Clin. Rev. Bone Miner. Metab. 13 (2015) 232–244. https://doi.org/10.1007/s12018-015-9194-9.

[2] A.-M. Yousefi, A review of calcium phosphate cements and acrylic bone cements as injectable materials for bone repair and implant fixation, J. Appl. Biomater. Funct. Mater. 17 (2019) 228080001987259. https://doi.org/10.1177/2280800019872594.

[3] G.C. Ingavle, M. Gionet-Gonzales, C.E. Vorwald, L.K. Bohannon, K. Clark, L.D. Galuppo, J.K. Leach, Injectable mineralized microsphere-loaded composite hydrogels for bone repair in a sheep bone defect model, Biomaterials. 197 (2019) 119–128. https://doi.org/10.1016/j.biomaterials.2019.01.005.

[4] Q. ul A. Malik, S. Iftikhar, S. Zahid, S.Z. Safi, A.F. Khan, M. Nawshad, S. Ghafoor, A.S. Khan, A. Tufail Shah, Smart injectable self-setting bioceramics for dental applications, Mater. Sci. Eng. C. 113 (2020) 110956. https://doi.org/10.1016/j.msec.2020.110956.

[5] W. Liu, J. Sun, Y. Sun, Y. Xiang, Y. Yan, Z. Han, W. Bi, F. Yang, Q. Zhou, L. Wang, Y. Yu, Multifunctional injectable protein-based hydrogel for bone regeneration, Chem. Eng. J. 394 (2020) 124875. https://doi.org/10.1016/j.cej.2020.124875.

[6] F. Guo, K. Huang, J. Niu, T. Kuang, Y. Zheng, Z. Gu, J. Zou, Enhanced osseointegration of double network hydrogels via calcium polyphosphate incorporation for bone regeneration, Int. J. Biol. Macromol. 151 (2020) 1126–1132. https://doi.org/10.1016/j.ijbiomac.2019.10.155.

[7] E.M. Ahmed, Hydrogel: Preparation, characterization, and applications: A review, J. Adv. Res. 6 (2015) 105–121. https://doi.org/10.1016/j.jare.2013.07.006.

[8] Z. Sun, S. Liu, K. Li, L. Tan, L. Cen, G. Fu, Well-defined and biocompatible hydrogels with toughening and reversible photoresponsive properties., Soft Matter. 12 (2016) 2192–2199. https://doi.org/10.1039/c5sm02129d.

[9] T.R. Hoare, D.S. Kohane, Hydrogels in drug delivery: Progress and challenges, Polymer (Guildf). 49 (2008) 1993–2007. https://doi.org/10.1016/j.polymer.2008.01.027.

[10] M.S. Saveleva, K. Eftekhari, A. Abalymov, T.E.L. Douglas, D. Volodkin, B. V. Parakhonskiy, A.G. Skirtach, Hierarchy of Hybrid Materials—The Place of Inorganics-in-Organics in it, Their Composition and Applications, Front. Chem. 7 (2019) 1–21. https://doi.org/10.3389/fchem.2019.00179.

[11] A.C. Hernández-González, L. Téllez-Jurado, L.M. Rodríguez-Lorenzob, SYNTHESIS OF IN-SITU SILICA-ALGINATE HYBRID HYDROGELS BY A SOL-GEL ROUTE, Carbohydr. Polym. 250 (2020) 116877. https://doi.org/10.1016/j.carbpol.2020.116877.

[12] T.E.L. Douglas, W. Piwowarczyk, E. Pamula, J. Liskova, D. Schaubroeck, S.C.G. Leeuwenburgh, G. Brackman, L. Balcaen, R. Detsch, H. Declercq, K. Cholewa-Kowalska, A. Dokupil, V.M.J.I. Cuijpers, F. Vanhaecke, R. Cornelissen, T. Coenye, A.R. Boccaccini, P. Dubruel, Injectable self-gelling composites for bone tissue engineering based on gellan gum hydrogel enriched with different bioglasses., Biomed. Mater. 9 (2014) 045014. https://doi.org/10.1088/1748-6041/9/4/045014.

[13] M.G. Manda, L.P. da Silva, M.T. Cerqueira, D.R. Pereira, M.B. Oliveira, J.F. Mano, A.P. Marques, J.M. Oliveira, V.M. Correlo, R.L. Reis, Gellan gum-hydroxyapatite composite spongy-like hydrogels for bone tissue engineering, J. Biomed. Mater. Res. Part A. 106 (2018) 479–490. https://doi.org/10.1002/jbm.a.36248.

[14] T. Douglas, M. Wlodarczyk, E. Pamula, H. Declercq, E. de Mulder, M. Bucko, L. Balcaen, F. Vanhaecke, R. Cornelissen, P. Dubruel, J. Jansen, S. Leeuwenburgh, Enzymatic mineralization of gellan gum hydrogel for bone tissue-engineering applications and its enhancement by polydopamine, J. Tissue Eng. Regen. Med. 8 (2014) 906–918. https://doi.org/10.1002/term.1616.

[15] T.E.L. Douglas, M. Pilarz, M. Lopez-Heredia, G. Brackman, D. Schaubroeck, L. Balcaen, V. Bliznuk, P. Dubruel, C. Knabe-Ducheyne, F. Vanhaecke, T. Coenye, E. Pamula, Composites of gellan gum hydrogel enzymatically mineralized with calcium-zinc phosphate for bone regeneration with antibacterial activity, J. Tissue Eng. Regen. Med. (2015) n/a-n/a. https://doi.org/10.1002/term.2062.

[16] A. Abalymov, L. Van Der Meeren, M. Saveleva, E. Prikhozhdenko, K. Dewettinck, B. Parakhonskiy, A.G. Skirtach, Cells-Grab-on Particles: A Novel Approach to Control Cell Focal Adhesion on Hybrid Thermally Annealed Hydrogels, ACS Biomater. Sci. Eng. 6 (2020) 3933–3944. https://doi.org/10.1021/acsbiomaterials.0c00119.

[17] M.A. Lopez-Heredia, A. Łapa, A.C. Mendes, L. Balcaen, S.K. Samal, F. Chai, P. Van der Voort, C. V. Stevens, B. V. Parakhonskiy, I.S. Chronakis, F. Vanhaecke, N. Blanchemain, E. Pamuła, A.G. Skirtach, T.E.L. Douglas, Bioinspired, biomimetic, double-enzymatic mineralization of hydrogels for bone regeneration with calcium carbonate, Mater. Lett. 190 (2017) 13–16. https://doi.org/10.1016/j.matlet.2016.12.122.

[18] E. Giuliano, D. Paolino, M.C. Cristiano, M. Fresta, D. Cosco, Rutin-Loaded Poloxamer 407-Based Hydrogels for In Situ Administration: Stability Profiles and Rheological Properties, Nanomaterials. 10 (2020) 1069. https://doi.org/10.3390/nano10061069.

[19] E. Lengert, A.M. Yashchenok, V. Atkin, A. Lapanje, D.A. Gorin, G.B. Sukhorukov, B. V. Parakhonskiy, Hollow silver alginate microspheres for drug delivery and surface enhanced Raman scattering detection, RSC Adv. 6 (2016) 20447–20452. https://doi.org/10.1039/C6RA02019D.

[20] E. Lengert, B. V. Parakhonskiy, D. Khalenkow, A. Zečić, M. Vangheel, J.M. Monje Moreno, B.P. Braeckman, A.G. Skirtach, Laser-induced remote release in vivo in C. elegans from novel silver nanoparticles-alginate hydrogel shells, Nanoscale. 10 (2018) 17249–17256. https://doi.org/10.1039/C8NR00893K.

[21] A.A. Abalymov, L. Van Poelvoorde, V. Atkin, A.G. Skirtach, M. Konrad, B. V. Parakhonskiy, Alkaline Phosphatase Delivery System Based on Calcium Carbonate Carriers for Acceleration of Ossification, ACS Appl. Bio Mater. 3 (2020) 2986–2996. https://doi.org/10.1021/acsabm.0c00053.

[22] K. Gkioni, S.C.G.G. Leeuwenburgh, T.E.L.L. Douglas, A.G. Mikos, J. a. Jansen, Mineralization of Hydrogels for Bone Regeneration, Tissue Eng. Part B. Rev. 16 (2010) 577–585. https://doi.org/10.1089/ten.teb.2010.0462.

[23] T. Douglas, Biomemetic Mineralisation of Hydrogel, in: C. Aparicio, M.-P. Ginebra (Eds.), Biominer. Biomater. Fundam. Appl., 2015: p. 482.

[24] S. Donatan, A. Yashchenok, N. Khan, B. V. Parakhonskiy, M. Cocquyt, B.-E. Pinchasik, D. Khalenkow, H. Möhwald, M. Konrad, A. Skirtach, Loading Capacity versus Enzyme Activity in Anisotropic and Spherical Calcium Carbonate Microparticles, ACS Appl. Mater. Interfaces. 8 (2016) 14284–14292. https://doi.org/10.1021/acsami.6b03492.

[25] D. V. Volodkin, S. Schmidt, P. Fernandes, N.I. Larionova, G.B. Sukhorukov, C. Duschl, H. Möhwald, R. von Klitzing, One-Step Formulation of Protein Microparticles with Tailored Properties: Hard Templating at Soft Conditions, Adv. Funct. Mater. 22 (2012) 1914–1922. https://doi.org/10.1002/adfm.201103007.

[26] Y.I. Svenskaya, H. Fattah, A.M. Zakharevich, D.A. Gorin, G.B. Sukhorukov, B. V. Parakhonskiy, Ultrasonically assisted fabrication of vaterite submicron-sized carriers, Adv. Powder Technol. 27 (2016) 618–624. https://doi.org/10.1016/j.apt.2016.02.014.

[27] S. Sovova, A. Abalymov, M. Pekar, A.G. Skirtach, B. Parakhonskiy, Calcium carbonate particles: synthesis, temperature and time influence on the size, shape, phase, and their impact on cell hydroxyapatite formation, J. Mater. Chem. B. 9 (2021) 8308–8320. https://doi.org/10.1039/D1TB01072G.

[28] B. V. Parakhonskiy, C. Foss, E. Carletti, M. Fedel, A. Haase, A. Motta, C. Migliaresi, R. Antolini, Tailored intracellular delivery via a crystal phase transition in 400 nm vaterite particles, Biomater. Sci. 1 (2013) 1273. https://doi.org/10.1039/c3bm60141b.

[29] Y. Svenskaya, B. V. Parakhonskiy, A. Haase, V. Atkin, E. Lukyanets, D. Gorin, R. Antolini, Anticancer drug delivery system based on calcium carbonate particles loaded with a photosensitizer, Biophys. Chem. 182 (2013) 11–15. https://doi.org/10.1016/j.bpc.2013.07.006.

[30] B. V. Parakhonskiy, A.M. Yashchenok, M. Konrad, A.G. Skirtach, Colloidal micro- and nano-particles as templates for polyelectrolyte multilayer capsules, Adv. Colloid Interface Sci. 207 (2014) 253–264. https://doi.org/10.1016/j.cis.2014.01.022.

[31] D.B. Trushina, T. V. Bukreeva, M. V. Kovalchuk, M.N. Antipina, CaCO3 vaterite microparticles for biomedical and personal care applications, Mater. Sci. Eng. C. 45 (2014) 644–658. https://doi.org/10.1016/j.msec.2014.04.050.

[32] B. V. Parakhonskiy, M. V Zyuzin, A. Yashchenok, S. Carregal-Romero, J. Rejman, H. Möhwald, W.J. Parak, A.G. Skirtach,

The influence of the size and aspect ratio of anisotropic, porous CaCO3 particles on their uptake by cells, J. Nanobiotechnology. 13 (2015) 53. https://doi.org/10.1186/s12951-015-0111-7.

[33] Y. Tarakanchikova, A. Muslimov, I. Sergeev, K. Lepik, N. Yolshin, A. Goncharenko, K. Vasilyev, I. Eliseev, A. Bukatin, V. Sergeev, S. Pavlov, A. Popov, I. Meglinski, B. Afanasiev, B. Parakhonskiy, G. Sukhorukov, D. Gorin, A highly efficient and safe gene delivery platform based on polyelectrolyte core–shell nanoparticles for hard-to-transfect clinically relevant cell types, J. Mater. Chem. B. 8 (2020) 9576–9588. https://doi.org/10.1039/D0TB01359E.

[34] Y.I. Svenskaya, H. Fattah, O.A. Inozemtseva, A.G. Ivanova, S.N. Shtykov, D.A. Gorin, B. V. Parakhonskiy, Key Parameters for Size- and Shape-Controlled Synthesis of Vaterite Particles, Cryst. Growth Des. 18 (2018) 331–337. https://doi.org/10.1021/acs.cgd.7b01328.

[35] D.B. Trushina, S.N. Sulyanov, T.V. Bukreeva, M.V. Kovalchuk, Size control and structure features of spherical calcium carbonate particles, Crystallogr. Reports. 60 (2015) 570–577. https://doi.org/10.1134/S1063774515040227.

[36] D. Preisig, D. Haid, F.J.O. Varum, R. Bravo, R. Alles, J. Huwyler, M. Puchkov, Drug loading into porous calcium carbonate microparticles by solvent evaporation, Eur. J. Pharm. Biopharm. 87 (2014) 548–558. https://doi.org/10.1016/J.EJPB.2014.02.009.

[37] C. Wang, C. He, Z. Tong, X. Liu, B. Ren, F. Zeng, Combination of adsorption by porous CaCO3 microparticles and encapsulation by polyelectrolyte multilayer films for sustained drug delivery., Int. J. Pharm. 308 (2006) 160–7. https://doi.org/10.1016/j.ijpharm.2005.11.004.

[38] J.R. Lakkakula, R. Kurapati, I. Tynga, H. Abrahamse, A.M.M. Raichur, R.W. Maçedo Krause, Cyclodextrin grafted calcium carbonate vaterite particles: efficient system for tailored release of hydrophobic anticancer or hormone drugs, RSC Adv. 6 (2016) 104537–104548. https://doi.org/10.1039/C6RA12951J.

[39] B. V Parakhonskiy, N.Y. Shilyagina, O.I. Gusliakova, A.B. Volovetskiy, A.B. Kostyuk, I. V Balalaeva, L.G. Klapshina, S.A. Lermontova, V. Tolmachev, A. Orlova, D.A. Gorin, G.B. Sukhorukov, A. V Zvyagin, A method of drug delivery to tumors based on rapidly biodegradable drug-loaded containers, Appl. Mater. Today. 25 (2021) 101199. https://doi.org/10.1016/j.apmt.2021.101199.

[40] Y.I. Svenskaya, A.M. Pavlov, D.A. Gorin, D.J. Gould, B. V. Parakhonskiy, G.B. Sukhorukov, Photodynamic therapy platform based on localized delivery of photosensitizer by vaterite submicron particles, Colloids Surfaces B Biointerfaces. 146 (2016) 171–179. https://doi.org/10.1016/j.colsurfb.2016.05.090.

[41] C. Peng, Q. Zhao, C. Gao, Sustained delivery of doxorubicin by porous CaCO3 and chitosan/alginate multilayers-coated CaCO3 microparticles, Colloids Surfaces A Physicochem. Eng. Asp. 353 (2010) 132–139. https://doi.org/10.1016/j.colsurfa.2009.11.004.

[42] S.A. Kamba, M. Ismail, S.H. Hussein-Al-Ali, T.A.T. Ibrahim, Z.A.B. Zakaria, In vitro delivery and controlled release of doxorubicin for targeting osteosarcoma bone cancer, Molecules. 18 (2013) 10580–10598. https://doi.org/10.3390/molecules180910580.

[43] J. Dou, F. Zhao, W. Fan, Z. Chen, X. Guo, Preparation of non-spherical vaterite CaCO3 particles by flash nano precipitation technique for targeted and extended drug delivery, J. Drug Deliv. Sci. Technol. 57 (2020) 1–8. https://doi.org/10.1016/j.jddst.2020.101768.

[44] C.K. Kuo, P.X. Ma, Ionically crosslinked alginate hydrogels as scaffolds for tissue engineering: Part 1. Structure, gelation rate and mechanical properties, Biomaterials. 22 (2001) 511–521. https://doi.org/10.1016/S0142-9612(00)00201-5.

[45] A. Sergeeva, R. Sergeev, E. Lengert, A. Zakharevich, B. V. Parakhonskiy, D. Gorin, S. Sergeev, D. V. Volodkin, Composite Magnetite and Protein Containing CaCO 3 Crystals. External Manipulation and Vaterite → Calcite Recrystallization-Mediated Release Performance, ACS Appl. Mater. Interfaces. 7 (2015) 21315–21325. https://doi.org/10.1021/acsami.5b05848.

[46] A.S. Sergeeva, D.A. Gorin, D. V. Volodkin, In-Situ Assembly of Ca-Alginate Gels with Controlled Pore Loading/Release Capability, Langmuir. 31 (2015) 10813–10821. https://doi.org/10.1021/acs.langmuir.5b01529.

[47] A. Sergeeva, N. Feoktistova, V. Prokopovic, D. Gorin, D. V. Volodkin, Design of Porous Alginate Hydrogels by Sacrificial CaCO3 Templates: Pore Formation Mechanism, Adv. Mater. Interfaces. 2 (2015) 1–10. https://doi.org/10.1002/admi.201500386.

[48] M.S. Saveleva, A.N. Ivanov, J.A. Chibrikova, A.A. Abalymov, M.A. Surmeneva, R.A. Surmenev, B. V. Parakhonskiy, M. V. Lomova, A.G. Skirtach, I.A. Norkin, Osteogenic Capability of Vaterite-Coated Nonwoven Polycaprolactone Scaffolds for In Vivo Bone Tissue Regeneration, Macromol. Biosci. (2021) 2100266. https://doi.org/10.1002/mabi.202100266.

[49] B. V. Parakhonskiy, A.M. Yashchenok, S. Donatan, D. V. Volodkin, F. Tessarolo, R. Antolini, H. Möhwald, A.G. Skirtach, Macromolecule Loading into Spherical, Elliptical, Star-Like and Cubic Calcium Carbonate Carriers, ChemPhysChem. 15 (2014) 2817–2822. https://doi.org/10.1002/cphc.201402136.

[50] J. Campbell, A.S. Vikulina, Layer-By-Layer Assemblies of Biopolymers: Build-Up, Mechanical Stability and Molecular Dynamics, Polymers (Basel). 12 (2020) 1949. https://doi.org/10.3390/polym12091949.

[51] E. V. Lengert, S.I. Koltsov, J. Li, A. V. Ermakov, B. V. Parakhonskiy, E. V. Skorb, A.G. Skirtach, Nanoparticles in Polyelectrolyte Multilayer Layer-by-Layer (LbL) Films and Capsules—Key Enabling Components of Hybrid Coatings, Coatings. 10 (2020) 1131. https://doi.org/10.3390/coatings10111131.

[52] D. Volodkin, A. Skirtach, H. Möhwald, Bioapplications of light-sensitive polymer films and capsules assembled using the layer-by-layer technique, Polym. Int. 61 (2012) 673–679. https://doi.org/10.1002/pi.4182.

[53] F. Mammoli, S. Castiglioni, S. Parenti, C. Cappadone, G. Farruggia, S. Iotti, P. Davalli, J.A.M. Maier, A. Grande, C. Frassineti, Magnesium is a key regulator of the balance between osteoclast and osteoblast differentiation in the presence of vitamin D 3, Int. J. Mol. Sci. 20 (2019) 1–17. https://doi.org/10.3390/ijms20020385.

[54] J.W. Park, Y.J. Kim, J.H. Jang, H. Song, Osteoblast response to magnesium ion-incorporated nanoporous titanium oxide surfaces, Clin. Oral Implants Res. 21 (2010) 1278–1287. https://doi.org/10.1111/j.1600-0501.2010.01944.x.

[55] H. Zreiqat, C.R. Howlett, A. Zannettino, P. Evans, G. Schulze-Tanzil, C. Knabe, M. Shakibaei, Mechanisms of magnesium-stimulated adhesion of osteoblastic cells to commonly used orthopaedic implants, J. Biomed. Mater. Res. 62 (2002) 175–184. https://doi.org/10.1002/jbm.10270.

[56] K.-J. Kim, S. Choi, Y. Sang Cho, S.-J. Yang, Y.-S. Cho, K.K. Kim, Magnesium ions enhance infiltration of osteoblasts in scaffolds via increasing cell motility, J. Mater. Sci. Mater. Med. 28 (2017) 96. https://doi.org/10.1007/s10856-017-5908-5.

[57] A. Abalymov, L. Van der Meeren, A.G. Skirtach, B. V. Parakhonskiy, Identification and Analysis of Key Parameters for the Ossification on Particle Functionalized Composites Hydrogel Materials, ACS Appl. Mater. Interfaces. 12 (2020) 38862–38872. https://doi.org/10.1021/acsami.0c06641.

[58] T.E.L. Douglas, A. Łapa, K. Reczyńska, M. Krok-Borkowicz, K. Pietryga, S.K. Samal, H.A. Declercq, D. Schaubroeck, M. Boone, P. Van der Voort, K. De Schamphelaere, C. V. Stevens, V. Bliznuk, L. Balcaen, B. V. Parakhonskiy, F. Vanhaecke, V. Cnudde, E. Pamuła, A.G. Skirtach, Novel injectable, self-gelling hydrogel–microparticle composites for bone regeneration consisting of gellan gum and calcium and magnesium carbonate microparticles, Biomed. Mater. 11 (2016) 065011. https://doi.org/10.1088/1748-6041/11/6/065011.

[59] T.E.L. Douglas, K. Sobczyk, A. Łapa, K. Włodarczyk, G. Brackman, I. Vidiasheva, K. Reczyńska, K. Pietryga, D. Schaubroeck, V. Bliznuk, P. Van Der Voort, H.A. Declercq, J. Van den Bulcke, S.K. Samal, D. Khalenkow, B. V. Parakhonskiy, J. Van Acker, T. Coenye, M. Lewandowska-Szumieł, E. Pamuła, A.G. Skirtach, Ca:Mg:Zn:CO 3 and Ca:Mg:CO 3 —tri- and bi-elemental carbonate microparticles for novel injectable self-gelling hydrogel–microparticle composites for tissue regeneration, Biomed. Mater. 12 (2017) 025015. https://doi.org/10.1088/1748-605X/aa6200.

[60] A.A. Abalymov, C.A.B. Santos, L. Van der Meeren, D. Van de Walle, K. Dewettinck, B. V. Parakhonskiy, A.G. Skirtach, Nanofibrillar Hydrogels by Temperature Driven Self-Assembly: New Structures for Cell Growth and Their Biological and Medical Implications, Adv. Mater. Interfaces. 8 (2021) 2002202. https://doi.org/10.1002/admi.202002202.

[61] T.E.L. Douglas, J.K. Keppler, M. Vandrovcová, M. Plencner, J. Beranová, M. Feuereisen, B. V. Parakhonskiy, Y. Svenskaya, V. Atkin, A. Ivanova, P. Ricquier, L. Balcaen, F. Vanhaecke, A. Schieber, L. Bačáková, A.G. Skirtach, Enhancement of Biomimetic Enzymatic Mineralization of Gellan Gum Polysaccharide Hydrogels by Plant-Derived Gallotannins, Int. J. Mol. Sci. 21 (2020) 2315. https://doi.org/10.3390/ijms21072315.

[62] A.A. Abalymov, L. Van Der Meeren, M. Saveleva, E. Prikhozhdenko, K. Dewettinck, B. V. Parakhonskiy, A.G. Skirtach, Cells-Grab-on Particles: A Novel Approach to Control Cell Focal Adhesion on Hybrid Thermally Annealed Hydrogels, ACS Biomater. Sci. Eng. 6 (2020) 3933–3944. https://doi.org/10.1021/acsbiomaterials.0c00119.

[63] H.J. Butt, B. Cappella, M. Kappl, Force measurements with the atomic force microscope: Technique, interpretation and

applications, Surf. Sci. Rep. 59 (2005) 1–152. https://doi.org/10.1016/j.surfrep.2005.08.003.

[64] J. Alcaraz, L. Buscemi, M. Grabulosa, X. Trepat, B. Fabry, R. Farré, D. Navajas, Microrheology of human lung epithelial cells measured by atomic force microscopy, Biophys. J. 84 (2003) 2071–2079. https://doi.org/10.1016/S0006-3495(03)75014-0.

[65] P. Sollich, F. Lequeux, P. Hébraud, M.E. Cates, Rheology of soft glassy materials, Phys. Rev. Lett. 78 (1997) 2020–2023. https://doi.org/10.1103/PhysRevLett.78.2020.

[66] A. Le Bail, S. Ouhenia, D. Chateigner, Microtwinning hypothesis for a more ordered vaterite model, Powder Diffr. 26 (2012) 16–21. https://doi.org/10.1154/1.3552994.

[67] A. Botha, C.A. Strydom, Dta and Ft-Ir Analysis of the Rehydration of Basic Magnesium Carbonate, J. Therm. A Nalysis Calorim. 71 (2003) 987–995. https://doi.org/10.1023/A:1023355016208.

[68] R. Kocen, M. Gasik, A. Gantar, S. Novak, Viscoelastic behaviour of hydrogel-based composites for tissue engineering under mechanical load, Biomed. Mater. 12 (2017) 25004. https://doi.org/10.1088/1748-605X/aa5b00.

[69] N. Devi, J. Dutta, Preparation and characterization of chitosan-bentonite nanocomposite films for wound healing application, Int. J. Biol. Macromol. 104 (2017) 1897–1904. https://doi.org/10.1016/j.ijbiomac.2017.02.080.

[70] F.A. Ruiz, C.R. Lea, E. Oldfield, R. Docampo, Human Platelet Dense Granules Contain Polyphosphate and Are Similar to Acidocalcisomes of Bacteria and Unicellular Eukaryotes, J. Biol. Chem. 279 (2004) 44250–44257. https://doi.org/10.1074/jbc.M406261200.

[71] W. Wang, K.W.K. Yeung, Bone grafts and biomaterials substitutes for bone defect repair: A review, Bioact. Mater. 2 (2017) 224–247. https://doi.org/10.1016/j.bioactmat.2017.05.007.

[72] I. Levental, P.C. Georges, P.A. Janmey, Soft biological materials and their impact on cell function, Soft Matter. 3 (2007) 299–306. https://doi.org/10.1039/B610522J.

[73] T.E.L. Douglas, M. Dziadek, J. Schietse, M. Boone, H.A. Declercq, T. Coenye, V. Vanhoorne, C. Vervaet, L. Balcaen, M. Buchweitz, F. Vanhaecke, F. Van Assche, K. Cholewa-Kowalska, A.G. Skirtach, Pectin-bioactive glass self-gelling, injectable composites with high antibacterial activity, Carbohydr. Polym. 205 (2019) 427–436. https://doi.org/10.1016/j.carbpol.2018.10.061.

[74] A.M. Kumar, A.Y. Adesina, M.A. Hussein, S.A. Umoren, S. Ramakrishna, S. Saravanan, Preparation and characterization of Pectin/Polypyrrole based multifunctional coatings on TiNbZr alloy for orthopaedic applications, Carbohydr. Polym. 242 (2020) 116285. https://doi.org/10.1016/j.carbpol.2020.116285.